Article

Developmental Cell

# Lysosomal Signaling Promotes Longevity by Adjusting Mitochondrial Activity

## Graphical Abstract

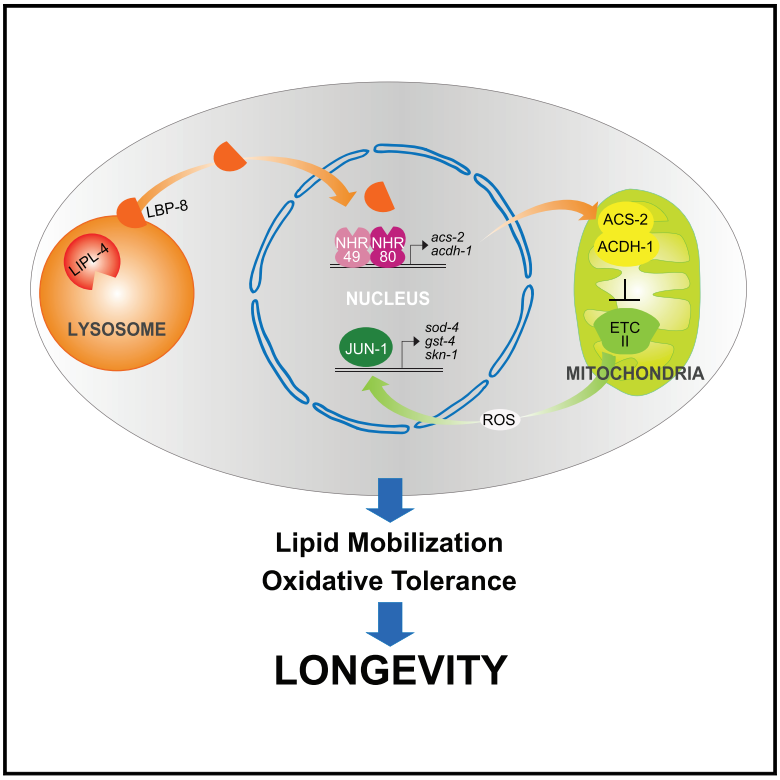


## Authors

Prasanna V. Ramachandran, Marzia Savini, Andrew K. Folick, Kuang Hu, Ruchi Masand, Brett H. Graham, Meng C. Wang

## Correspondence

wmeng@bcm.edu

## In Brief

Ramachandran et al. uncover in *C. elegans* metabolic and signaling inter-organelle communication between lysosomes, mitochondria, and the nucleus. They demonstrate a crucial role for lysosomal lipid messenger signaling to actively trigger adjustments in mitochondrial activity that in turn coordinate lipid metabolism, redox homeostasis, and longevity.

## Highlights

- Lysosomal lipid messenger signaling actively regulates mitochondrial ß-oxidation
- Mitochondrial ß-oxidation modulates electron transport chain complex II activity
- Lysosomal and mitochondrial pro-longevity signaling converge on JUN-1
- Organelle coordination improves metabolic balance, redox homeostasis, and longevity

Ramachandran et al., 2019, Developmental Cell *48*, 1–12
March 11, 2019 
https://doi.org/10.1016/j.devcel.2018.12.022

CellPress

Please cite this article in press as: Ramachandran et al., Lysosomal Signaling Promotes Longevity by Adjusting Mitochondrial Activity, Developmental Cell (2018), https://doi.org/10.1016/j.devcel.2018.12.022

Developmental Cell
Article



# Lysosomal Signaling Promotes Longevity by Adjusting Mitochondrial Activity

Prasanna V. Ramachandran,[1,2,4,6] Marzia Savini,[3,6] Andrew K. Folick,[3,4,6] Kuang Hu,[2] Ruchi Masand,[1] Brett H. Graham,[1,7] and Meng C. Wang[1,2,5,8,*]
[1]Department of Molecular and Human Genetics, Baylor College of Medicine, Houston, TX 77030, USA
[2]Huffington Center on Aging, Baylor College of Medicine, Houston, TX 77030, USA
[3]Program in Developmental Biology, Baylor College of Medicine, Houston, TX 77030, USA
[4]Medical Scientist Training Program, Baylor College of Medicine, Houston, TX 77030, USA
[5]Howard Hughes Medical Institute, Baylor College of Medicine, Houston, TX 77030, USA
[6]These authors contributed equally
[7]Present address: Department of Medical and Molecular Genetics, Indiana University School of Medicine, Indianapolis, IN 46202, USA
[8]Lead Contact
*Correspondence: wmeng@bcm.edu
https://doi.org/10.1016/j.devcel.2018.12.022

## SUMMARY

**Lysosomes and mitochondria are both crucial cellular organelles for metabolic homeostasis and organism health. However, mechanisms linking their metabolic activities to promote organism longevity remain poorly understood. We discovered that the induction of specific lysosomal signaling mediated by a LIPL-4 lysosomal acid lipase and its lipid chaperone LBP-8 increases mitochondrial ß-oxidation to reduce lipid storage and promote longevity in *Caenorhabditis elegans*. We further discovered that increased mitochondrial ß-oxidation reduces mitochondrial electron transport chain complex II activity, contributing to the induction of reactive oxygen species in mitochondria (mtROS) and the longevity effect conferred by LIPL-4–LBP-8 signaling. Moreover, by activating the JUN-1 transcription factor downstream of mtROS, the LIPL-4–LBP-8 signaling pathway induces antioxidant targets and oxidative stress tolerance. Together, these results reveal regulatory mechanisms by which lysosomal signaling triggers adjustments in mitochondrial activity and suggest the significance of these metabolic adjustments for improving metabolic fitness, redox homeostasis, and longevity.**

## INTRODUCTION

Metabolic activity is at the nexus of cellular homeostasis, and its dysregulation occurs during the aging process and underlies a wide variety of human diseases. For all eukaryotic cells, organelle compartmentation is a crucial component of metabolic regulation. Separation of metabolic pathways within different cellular organelles ensures metabolic specificity and efficiency, but at the same time, coordinated communication across specialized organelles is required to maintain cellular homeostasis and organismal fitness. Lysosomes and mitochondria are two of the most metabolically active cellular organelles, both playing critical roles in regulating metabolic health and organism longevity (Balaban et al., 2005; Rajawat et al., 2009; Ristow and Zarse, 2010; Settembre et al., 2013).

Lysosomes are loaded with various hydrolytic enzymes that digest endocytic and phagocytic cargoes from the environment (Luzio et al., 2007). Lysosomal hydrolysis is also essential for autophagy to degrade dysfunctional cellular components and maintain cellular integrity (Levine and Kroemer, 2008), which can be induced in various genetic, pharmacological, and dietary models of longevity as a prerequisite for their beneficial effects (Hansen et al., 2018). Importantly, not only are various structural building blocks and energy intermediates generated through lysosomal hydrolysis, but the metabolic state of the lysosome also impacts nuclear transcription and signal transduction (Folick et al., 2015; Settembre et al., 2013). Lysosomal amino acid levels can be sensed by mTORC1 that consequently regulates nuclear translocation of the transcription factor TFEB (Saxton and Sabatini, 2017; Settembre et al., 2013), and both mTORC1 and TFEB have been implicated in the regulation of longevity (Johnson et al., 2013; Kennedy and Lamming, 2016; Lapierre et al., 2013). On the other hand, we have discovered a lysosome-to-nucleus retrograde lipid messenger signaling pathway that promotes longevity in *C. elegans*, and this lysosomal signaling is triggered by a lysosomal lipase LIPL-4 and consequently induces a lipid chaperone protein LBP-8 and a lipid messenger oleoylethanolamide to activate nuclear gene expression (Folick et al., 2015).

Meanwhile, mitochondria constitute the powerhouse of the cell and coordinate fatty acid oxidation, the citric acid cycle, and oxidative phosphorylation via the electron transport chain (ETC). Mitochondrial ß-oxidation plays crucial roles in lipid catabolism. Following lipid hydrolysis, non-esterified free fatty acids are converted into acetyl-CoA through ß-oxidation cycles in mitochondria, and acetyl-CoA in turn enters the citric acid cycle for complete oxidation. Thus, tightly coupled activities between mitochondrial ß-oxidation and lipolysis ensure effective energy production and metabolic homeostasis. On the other hand, mitochondrial ß-oxidation and the citric acid cycle are closely connected with mitochondrial ETC. NADH and FADH2 generated from both mitochondrial ß-oxidation and the citric acid cycle

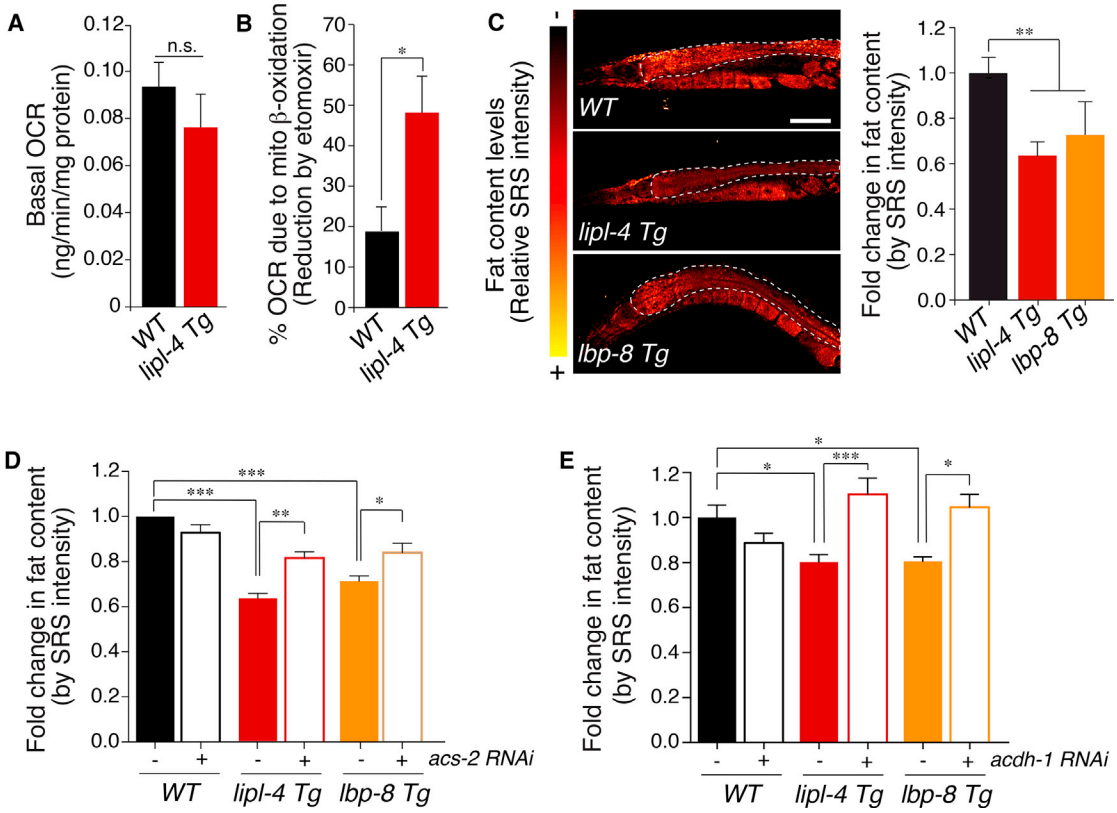


**Figure 1. Lysosomal Signaling Induces Mitochondrial ß-Oxidation and Fat Mobilization**

(A and B) Compared with wild-type (WT) animals, *C. elegans* transgenic strains overexpressing *lipl-4* (*lipl-4 Tg*) show increased mitochondrial ß-oxidation-dependent oxygen consumption. The oxygen consumption rate (OCR) is measured with a Seahorse XF24 Analyzer at baseline (A), and after the addition of the mitochondrial ß-oxidation inhibitor etomoxir, the percent decrease in OCR following etomoxir addition is shown (B). n = 200 for each genotype in 10 technical replicates. Error bars represent mean ± standard error of the mean (SEM) *p < 0.05, n.s. p > 0.05, Student's t test.

(C) Compared with WT, *lipl-4 Tg* and *C. elegans* transgenic strains overexpressing *lbp-8* (*lbp-8 Tg*) have reduced fat content levels. Fat storage is visualized by Stimulated Raman Scattering (SRS) microscopy, and the average signal intensity in anterior intestinal cells is quantified (Ramachandran et al., 2015). Scale bar, 50 μm. n = 20 for each genotype in 3 biological replicates. Error bars represent mean ± SEM. **p < 0.01, Student's t test.

(D) Reduction of fat content levels in *lipl-4 Tg* and *lbp-8 Tg* is suppressed by RNAi knockdown of *acs-2*, the acyl-coA synthetase. n = 20 for each genotype/condition in 3 biological replicates. Error bars represent mean ± SEM. ***p < 0.001, **p < 0.01, *p < 0.05, two-way ANOVA with Holm-Sidak correction.

(E) Reduced fat content in *lipl-4 Tg* and *lbp-8 Tg* is suppressed by RNAi knockdown of the acyl-coA dehydrogenase *acdh-1*. n = 20 for each genotype or condition in 3 biological replicates. Error bars represent mean ± SEM. ***p < 0.001, *p < 0.05, two-way ANOVA with Holm-Sidak correction.

See also Figure S1.

donate electrons to ETC for ATP production. Among the four protein complexes in ETC, complex II is the only one that participates in both the citric acid cycle and ETC by oxidizing succinate and reducing ubiquinone, respectively (Bezawork-Geleta et al., 2017). Interestingly, reduction in specific ETC functions has been associated with the regulation of longevity in *C. elegans*, *Drosophila*, and mice (Wang and Hekimi, 2015), which is likely associated with the signaling activity of mitochondria. Upon functional alterations in mitochondria, retrograde signaling can exploit different transcription factors to trigger specific gene expression changes in the nucleus (Quirós et al., 2016). For example, defective mitochondrial proteostasis activates mitochondrial unfolded protein response ($UPR^{mt}$) that induces the transcription of nuclear-encoded mitochondrial chaperone genes (Pellegrino et al., 2013), and the induction of $UPR^{mt}$ has been associated with the longevity effects conferred by reducing mitochondrial ETC functions (Lin and Haynes, 2016). Mitochondrial reactive oxygen species (mtROS)-mediated mitochondrial signaling is another crucial mechanism underlying the longevity regulation (Shadel and Horvath, 2015). Functional attenuation of mitochondrial ETC leads to increased production of mtROS (Lee et al., 2010; Yang and Hekimi, 2010), which is known to activate key signaling factors of different longevity pathways, such as the hypoxia inducible factor (HIF), the c-Jun N-terminal kinase (JNK), and the AMP activated protein kinase (AMPK) (Burkewitz et al., 2014; Hwang and Lee, 2011; Hwang et al., 2014; Sena and Chandel, 2012; Wang et al., 2003). Although ETC complex I and III are conventionally recognized as the major sites for mtROS production, complex II also contributes to ROS generation from both forward- and reverse-electron flux (Bezawork-Geleta et al., 2017; Wong et al., 2017).

In this work, we demonstrate that the LIPL-4–LBP-8 lysosomal lipid messenger signaling pathway actively promotes mitochondrial ß-oxidation, which specifically reduces ETC complex II and

Please cite this article in press as: Ramachandran et al., Lysosomal Signaling Promotes Longevity by Adjusting Mitochondrial Activity, Developmental Cell (2018), https://doi.org/10.1016/j.devcel.2018.12.022



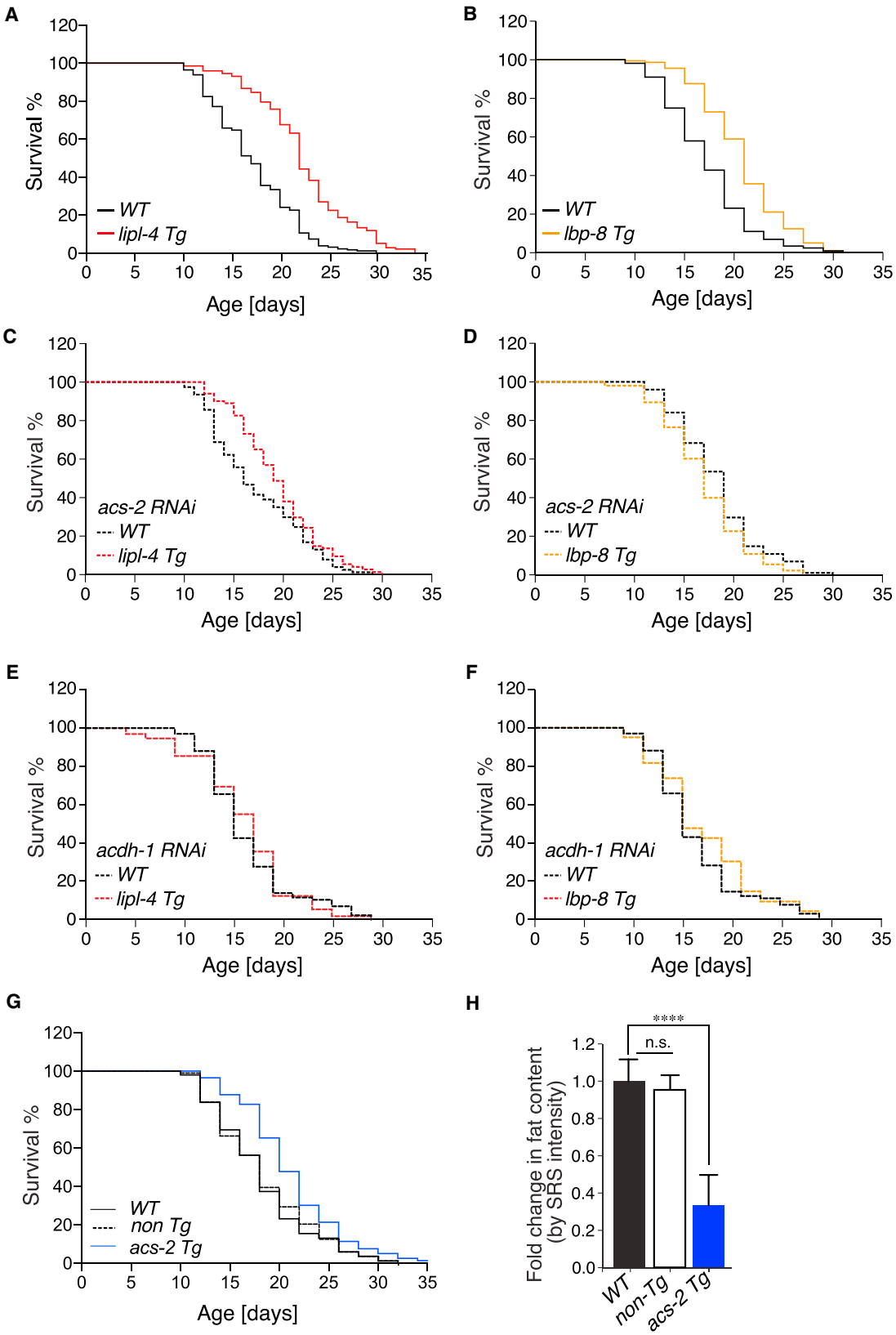


(legend on next page)

induces mtROS-mediated mitochondrial retrograde signaling. Together, these metabolic adjustments and signaling events improve lipid catabolism and stress tolerance, leading to increased longevity.

## RESULTS

### Lysosomal Signaling Promotes Fat Mobilization via Inducing Mitochondrial β-Oxidation

Induction of lysosomal lipolysis by constitutively expressing a lysosomal acid lipase, *lipl-4*, can trigger the translocation of signaling molecules, including the lipid chaperone *lbp-8* and the lipid messenger oleoylethanolamine, into the nucleus to transcriptionally activate metabolic genes (Folick et al., 2015). Two of these transcriptional targets, *acs-2* and *acdh-1*, encode acyl-CoA synthase and acyl-CoA dehydrogenase, respectively. Interestingly, both ACS-2 and ACDH-1 are localized at mitochondria and required for fatty acid β-oxidation. Given their induction in *lipl-4*-overexpressing transgenic animals (*lipl-4 Tg*) (Folick et al., 2015) (Figure S1A), we asked whether mitochondrial β-oxidation is indeed increased upon the induction of lysosomal lipolysis. We measured the oxygen consumption rate (OCR) in wild-type animals (WT) and *lipl-4 Tg* in the presence or absence of the mitochondrial β-oxidation inhibitor etomoxir. We found that the basal OCR is indistinguishable between WT and *lipl-4 Tg* (Figure 1A); however, a greater percentage of OCR reduction is detected in *lipl-4 Tg* upon etomoxir inhibition, suggesting an induction of mitochondrial β-oxidation in *lipl-4 Tg* compared to WT (Figure 1B).

Mitochondrial β-oxidation is an essential step during lipid catabolism, which breaks down fatty acid molecules in mitochondria to generate acetyl-CoA entering the citric acid cycle. Consistent with induced mitochondrial β-oxidation, we found that total fat storage in the intestine, the major fat storage tissue of *C. elegans* and the expression tissue for *lipl-4* and *lbp-8* (Folick et al., 2015), is reduced in *lipl-4 Tg* (Figure 1C), as well as in animals overexpressing the lipid chaperone *lbp-8* (*lbp-8 Tg*) (Figure 1C). Furthermore, when mitochondrial β-oxidation is inhibited by RNAi knockdown of *acs-2* or *acdh-1*, the reduced fat storage is suppressed in both *lipl-4 Tg* and *lbp-8 Tg* (Figures 1D and 1E). Together, these results show that the activation of the LIPL-4–LBP-8 lysosomal signaling pathway triggers fat mobilization by up-regulating mitochondrial β-oxidation.

### Increased Mitochondrial β-Oxidation Contributes to Organism Longevity

The LIPL-4–LBP-8 lysosomal signaling pathway plays a crucial role in regulating organism longevity, and both *lipl-4 Tg* and *lbp-8 Tg* are long-lived compared to WT (Folick et al., 2015; Wang et al., 2008). We next examined whether the induction of mitochondrial β-oxidation by LIPL-4 and LBP-8 is associated with their longevity effects. We found that RNAi inactivation of either *acs-2* or *acdh-1* suppresses the lifespan extension in *lipl-4 Tg* and *lbp-8 Tg* but does not affect WT lifespan (Figures 2A–2F; Table S1), suggesting that increased mitochondrial β-oxidation is necessary for the longevity-promoting effects conferred by the lysosomal signaling pathway. Moreover, the induction of mitochondrial β-oxidation by overexpressing *acs-2* specifically in the intestine (*acs-2 Tg*), the fat storage tissue of *C. elegans*, is sufficient to prolong lifespan (Figure 2G; Table S2) and reduce fat storage (Figure 2H). Together, these results suggest a link between lysosomes and mitochondria in regulating organism longevity.

### Lysosomal Signaling Regulates Mitochondrial ETC Activities

To further investigate the effect of lysosomal signaling on mitochondrial homeostasis, we analyzed mitochondrial content levels, $UPR^{mt}$ induction, and ETC activities in *lipl-4 Tg* and *lbp-8 Tg*. We found that the mitochondrial content level is unaltered in either transgenic strain (Figure 3A). Neither *lipl-4 Tg* nor *lbp-8 Tg* induces the transcriptional expression of mitochondrial chaperones *hsp-6* and *hsp-60* (Figure 3B), suggesting a negligible effect of lysosomal signaling on $UPR^{mt}$. On the other hand, we found that the enzymatic activity of mitochondrial ETC complex II, succinate dehydrogenase, but not the other complexes is reduced in both *lipl-4 Tg* and *lbp-8 Tg* (Figure 3C). Interestingly, inactivation of the mitochondrial β-oxidation genes, *acs-2* or *acdh-1*, restores the complex II activity in both transgenic strains (Figures 3D and 3E), suggesting the reduced complex II activity as a result of increased mitochondrial β-oxidation. In supporting this, induced mitochondrial β-oxidation in *acs-2 Tg* leads to a reduction in the complex II activity (Figure 3F), which recapitulates the effects conferred by *lipl-4 Tg* and *lbp-8 Tg*. Interestingly, succinate dehydrogenase functions in both the citric acid cycle and ETC by oxidizing succinate to fumarate and reducing ubiquinone to ubiquinol, respectively. Thus, by modulating the activity of succinate dehydrogenase and consequently the metabolic coupling between mitochondrial β-oxidation and respiratory chain activities, the LIPL-4–LBP-8 lysosomal signaling pathway might interact with mitochondrial ETC to regulate longevity.

### Lysosomal Signaling Interacts with Mitochondrial ETC to Regulate Longevity

Perturbing mitochondrial ETC functions is a conserved mechanism to extend lifespan across different species (Wang and

**Figure 2. Lysosomal Signaling Promotes Longevity through Inducing Mitochondrial ß-Oxidation**

(A and B) Compared with WT, both *lipl-4 Tg* and *lbp-8 Tg* exhibit extended lifespan ($p < 0.001$, log-rank test).

(C and D) RNAi knockdown of *acs-2* partially and fully suppresses the longevity of *lipl-4 Tg* (C) and *lbp-8 Tg* (D), respectively. ($p < 0.001$, RNAi versus ctrl for *Tg* animals, log-rank test). WT lifespan is unaffected by *acs-2* RNAi knockdown ($p < 0.05$, log-rank test). n = 60–100 for each genotype/condition.

(E and F) RNAi knockdown of *acdh-1* fully suppresses the longevity of both *lipl-4 Tg* (E) and *lbp-8 Tg* (F). ($p < 0.001$, RNAi versus ctrl for *Tg* animals, log-rank test). WT lifespan is unaffected by *acdh-1* RNAi knockdown ($p < 0.05$, log-rank test). n = 60–100 for each genotype/condition.

(G) Compared with WT and non-transgenic siblings, transgenic animals carrying *acs-2* overexpression specifically in the intestine, the fat storage tissue of *C. elegans* (*acs-2 Tg*), live longer ($p < 0.001$, log-rank test). n = 60–100 for each genotype/condition

(H) Compared with WT and non-transgenic siblings, *acs-2 Tg* show decreased fat content level. n = 20 for each genotype in 3 biological replicates. Error bars represent mean ± SEM. ***$p < 0.001$, one-way ANOVA, Holm-Sidak correction.

See also Tables S1 and S2 for lifespan data.

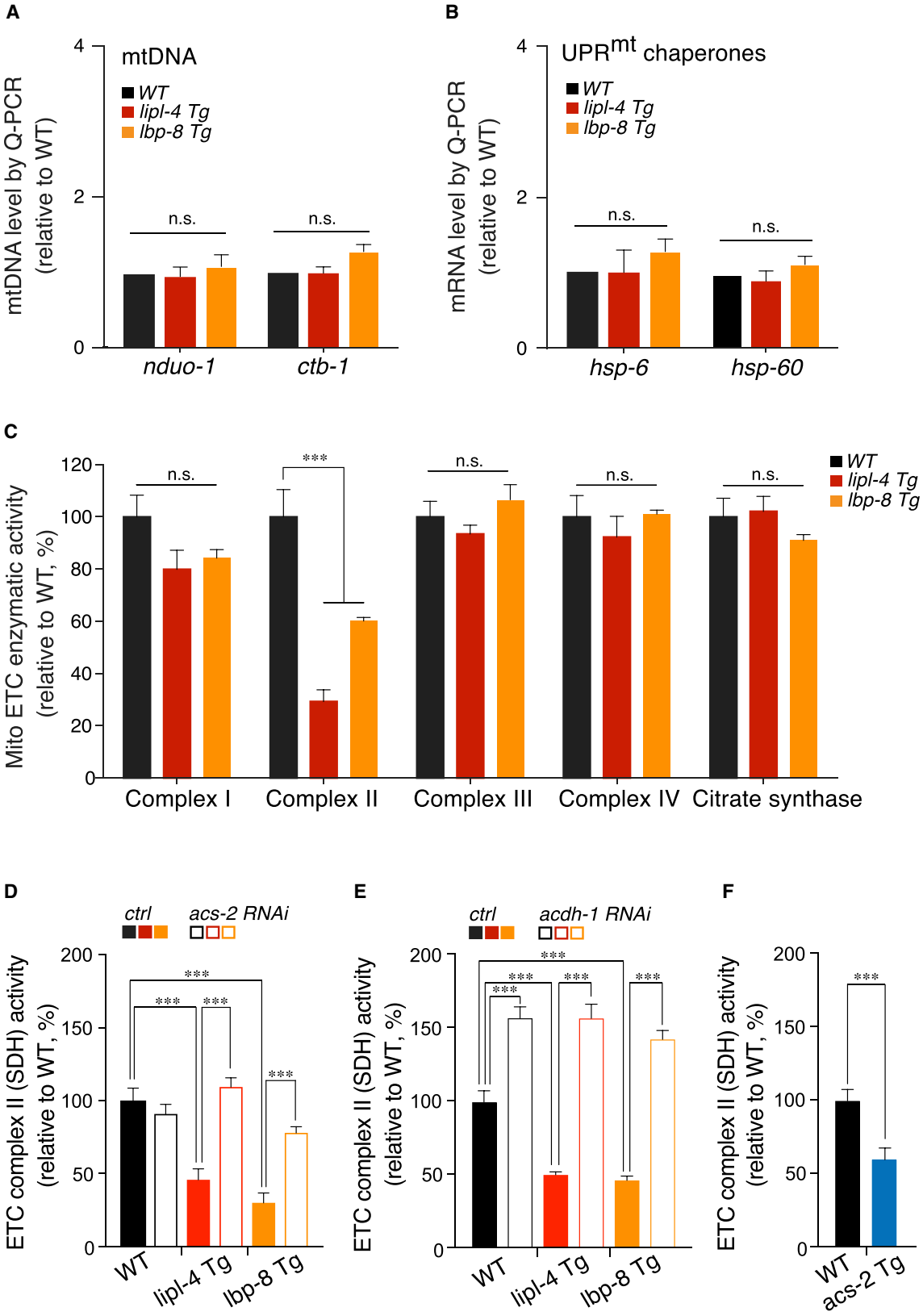


*(legend on next page)*

Hekimi, 2015). In *C. elegans, nuo-4* encodes the NADH ubiquinone oxidoreductase subunit of ETC complex I; *isp-1* encodes the Rieske iron sulfur protein subunit of complex III; *cco-1* encodes the cytochrome c oxidase-1 subunit Vb/COX4, a component of complex IV; and *clk-1* encodes a COQ7 homolog required for normal synthesis of ubiquinone. Inactivation of each of these mitochondrial genes significantly extends lifespan (Dillin et al., 2002; Felkai et al., 1999; Feng et al., 2001; Hamilton et al., 2005; Hansen et al., 2005; Lee et al., 2003) (Figures 4 and S2; Tables S1 and S2). On the other hand, *mev-1* encodes the succinate dehydrogenase cytochrome *b560* subunit of complex II, and its inactivation shortens *C. elegans* lifespan (Wang and Hekimi, 2015) (Figures 4E and 4F; Table S1). To confirm whether the lysosomal signaling pathway interacts with mitochondrial ETC to regulate longevity, we measured the lifespans of *lipl-4 Tg* and *lbp-8 Tg* in the background with different mitochondrial inactivations. We found that *lbp-8 Tg* loses its longevity-promoting effect when *nuo-4, mev-1*, *isp-1*, or *cco-1* is inactivated (Figures 4B, 4D, 4F, 4H, 4J, S2A, and S2E; Tables S1 and S2), but can further enhance the lifespan extension conferred by the inactivation of *clk-1* (Figures S2A and S2C; Table S2). On the other hand, we found that *lipl-4 Tg* cannot extend lifespan upon *mev-1* inactivation or further enhance the lifespan extension conferred by *isp-1* inactivation (Figures 4A, 4E, 4G, S2B, and S2F; Tables S1 and S2); however, in the background of *nuo-4*, *cco-1*, or *clk-1* inactivation *lipl-4 Tg* can still extend lifespan as effectively as in WT conditions (Figures 4A, 4C, 4I, S2B, and S2D; Tables S1 and S2). Together, these results suggest that LIPL-4–LBP-8 lysosomal signaling functions through mitochondrial ETC to regulate longevity. LBP-8 interacts with complex I–IV; however, LIPL-4 may have additional downstream effectors besides LBP-8 that interact selectively with complex II and III, but not I or IV.

## Lysosomal and Mitochondrial ETC Longevity Mechanisms Converge on JUN-1

The uncovering of this previously unknown interaction between mitochondrial ETC and lysosomal longevity mechanisms led us to further explore downstream mediators. Seven transcription factors have been previously associated with the longevity effect conferred by mitochondrial ETC reduction, including *taf-4*, *hif-1, aha-1*, *nhr-27*, *nhr-49*, *ceh-18*, and *jun-1* (Khan et al., 2013). We have demonstrated that *nhr-49*, which mediates the induction of *acs*-2, is fully required for the longevity of *lipl-4 Tg* and *lbp-8 Tg* (Folick et al., 2015). Here, we inactivated the other six transcription factors by RNAi and analyzed their effects on *lipl-4 Tg*- and *lbp-8 Tg*-mediated longevity (Figure 5; Table S1). We found that the inactivation of *taf-4* (Figures 5C and 5D; Table S1), *hif-1* (Figures 5E and 5F; Table S1), or *aha-1* (Figures 5G and 5H; Table S1) does not affect the lifespan-extending effect of either *lipl-4 Tg* or *lbp-8 Tg*. *ceh-18* inactivation extends the lifespan of WT, and this lifespan extension can be further enhanced in *lipl-4 Tg* and *lbp-8 Tg* (Figures 5I and 5J; Table S1). The inactivation of *nhr-27* suppresses the lifespan extension in *lbp-8 Tg* but has no effect on that in *lipl-4 Tg* (Figures 5K and 5L; Table S1). Interestingly, only knockdown of the *jun-1* transcription factor fully suppresses the longevity of both *lipl-4 Tg* and *lbp-8 Tg* (Figures 5M and 5N; Table S1), and the *jun-1* expression level is increased in *lipl-4 Tg* and *lbp-8 Tg* (Figure S3). Together, these results suggest that the lysosomal and mitochondrial ETC longevity mechanisms converge on the *jun-1* transcription factor.

## Lysosomal Signaling Induces mtROS and Improves Oxidative Stress Tolerance via JUN-1

*jun-1* encodes a homolog of the c-Jun transcription factor (Hiatt et al., 2009). c-Jun and c-Fos form the (activator protein 1) AP-1 transcription factor and mediate the transcriptional effects of the Jun N-terminal kinase (JNK) signaling pathway. The activation of JNK signaling is a key mechanism responding to ROS stimuli, which defends cells against oxidative damages and promotes longevity in both *C. elegans* and *Drosophila* (Uno et al., 2013; Wang et al., 2003). Interestingly, we found that mtROS production is increased in the long-lived *lipl-4 Tg* and *lbp-8 Tg*, and these inductions are suppressed when mitochondrial ß-oxidation is attenuated by *acs-2* RNAi (Figures 6A and 6B). Furthermore, we found that oxidative stress responsive genes are induced in *lipl-4 Tg* and *lbp-8 Tg* in a *jun-1* dependent manner, including glutathione S-transferase *gst-4* (Figure 6C) and superoxide dismutase *sod-4* (Figure 6D); and *acs-2* RNAi inactivation suppresses the induction of these antioxidant genes (Figures 6C and 6D). These results suggest that the active regulation of mitochondrial ß-oxidation by lysosomal signaling is critical for redox homeostasis. In support of this, we discovered that *skn-1*, the *C. elegans* homolog of the key antioxidant defense mediator Nrf2 (An and Blackwell, 2003; Blackwell et al., 2015), is induced in *lipl-4 Tg* and *lbp-8 Tg*, and the induction is dependent on *jun-1* (Figure 6E). Furthermore, we found that both *lipl-4 Tg* and *lbp-8 Tg* show increased resistance to oxidative damages induced by paraquat treatments (Figure 6F), and RNAi inactivation of

**Figure 3. Lysosomal Pro-longevity Signaling Selectively Alters Mitochondrial ETC Activities**

(A) Neither *lipl-4 Tg* nor *lbp-8 Tg* show changes in mitochondrial DNA content, measured by the levels of mitochondrial encoded genes *nduo-1* and *ctb-1*. n = 1,000 for each genotype in 3 biological replicates. Error bars represent mean ± SEM. n.s. $p > 0.05$, one-way ANOVA, Holm-Sidak correction.

(B) *lipl-4 Tg* and *lbp-8 Tg* do not transcriptionally activate *hsp-6* or *hsp-60*, two mitochondrial chaperones induced by $UPR^{mt}$. n = 1,000 for each genotype in 3 biological replicates. Error bars represent mean ± SEM. n.s. $p > 0.05$, one-way ANOVA, Holm-Sidak correction.

(C) Enzymatic activities of mitochondrial ETC complexes I (NADH:ubiquinone oxidoreductase), II (succinate dehydrogenase), III (ubiquinol:cytochrome c oxidoreductase), and IV (cytochrome c oxidase), as well as citrate synthase, are tested in *lipl-4 Tg* and *lbp-8 Tg* and normalized to WT levels. Only the activity of complex II (succinate dehydrogenase) is decreased in both *lipl-4 Tg* and *lbp-8 Tg*. n = 20,000 for each genotype in 10 technical replicates. Error bars represent mean ± SEM. ***$p < 0.001$, n.s. $p > 0.05$, two-way ANOVA, Holm-Sidak correction.

(D and E) Reduced activity of ETC complex II (succinate dehydrogenase) in *lipl-4 Tg* or *lbp-8 Tg* is suppressed upon reduction of mitochondrial ß-oxidation by *acs-2* (D) and *acdh-1* (E) RNAi knockdown. n = 1,000 for each genotype/condition in 3 biological replicates. Error bars represent mean ± SEM. ***$p < 0.001$, one-way ANOVA, Holm-Sidak correction.

(F) Compared with WT, *acs-2 Tg* shows decreased enzymatic activity of complex II (succinate dehydrogenase). n = 1,000 for each genotype/condition in 3 biological replicates. Error bars represent mean ± SEM. ***$p < 0.001$, unpaired t test, two-tailed method.

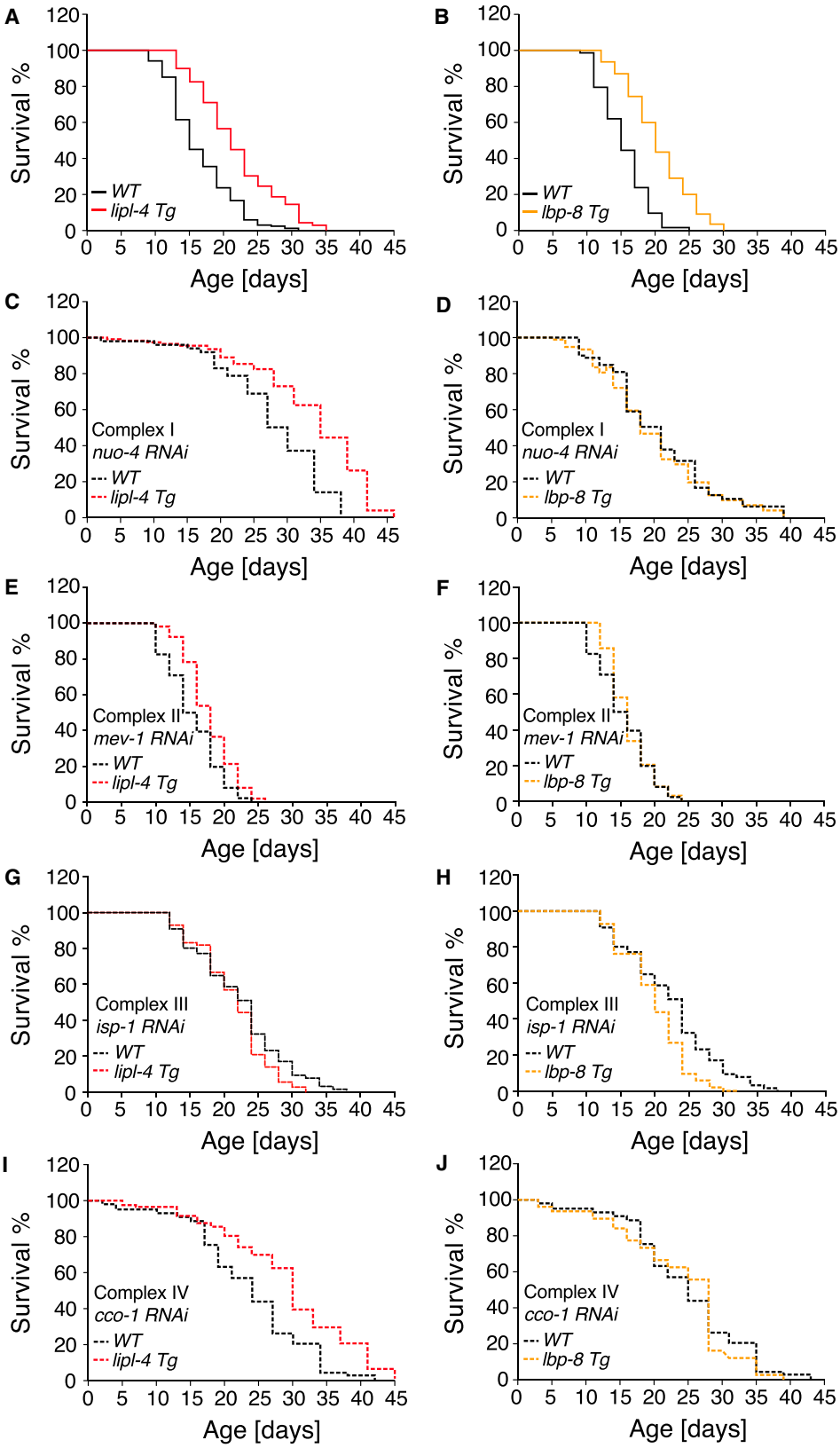


(legend on next page)

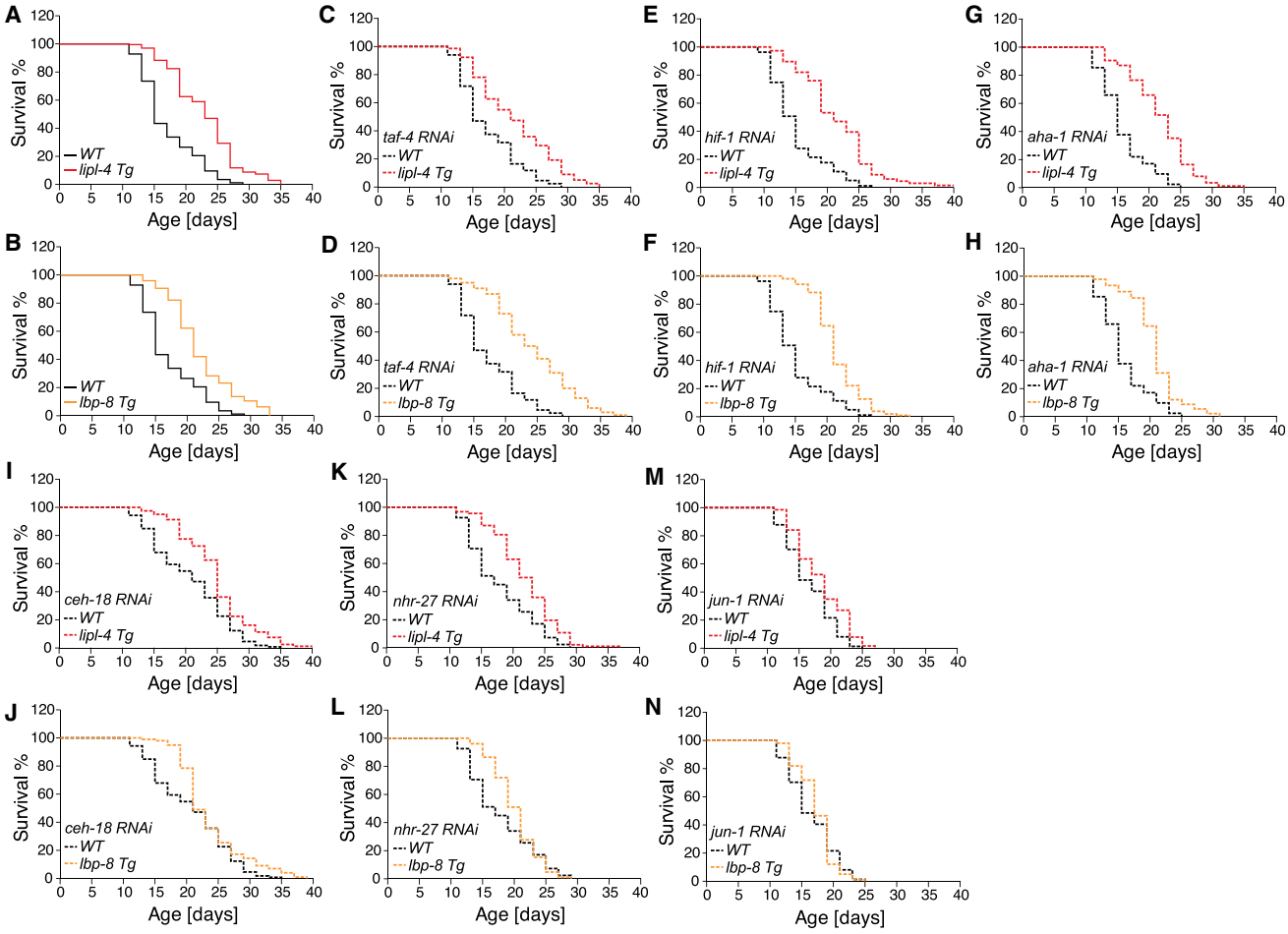


**Figure 5. Lysosomal Pro-longevity Signaling Acts through JUN-1 Transcription Factor**

(A–N) Lifespans of *lipl-4 Tg* (A, C, E, G, I, K, and M) and *lbp-8 Tg* (B, D, F, H, J, L, and N) are measured in the background of *taf-4* (C and D), *hif-1* (E and F), *aha-1* (G and H), *ceh-18* (I and J), *nhr-27* (K and L), or *jun-1* (M and N) inactivation by RNAi knockdown. Only *jun-1* (c-Jun homolog) inactivation fully suppresses the longevity of both *lipl-4 Tg* and *lbp-8 Tg* ($p < 0.05$ *Tg* versus WT with RNAi, log-rank test). n = 60–100 for each genotype/condition.

See also Table S1 for lifespan data.

*skn-1* fully suppresses the lifespan extension conferred by either *lipl-4* or *lbp-8 Tg* (Figures 6G and 6H). Together, these results suggest that by modulating mitochondrial metabolic activity, the lysosomal longevity pathway promotes mtROS production and consequently activates JNK signaling to improve redox homeostasis and longevity.

## DISCUSSION

In summary, our work uncovers a pathway by which lysosomal lipolysis actively regulates mitochondrial ß-oxidation to influence specific ETC activity, and lysosomal and mitochondrial signaling cooperate to modulate lipid metabolism and organism fitness (Figure 7). Glycolysis and lipolysis are basic catabolic processes for energy release that are mutually exclusive of each other (McGarry, 2002; Randle, 1998). As suggested by the glucose and fatty acid cycle, there is a reciprocal relationship between the oxidation of these two fuels. Upon activation of the LIPL-4–LBP-8 lysosomal longevity pathway, fatty acid β-oxidation is increased without affecting total metabolic rates, suggesting a switch in the preference of oxidation substrates from glucose to lipids. Interestingly, this metabolic switch has also been

**Figure 4. Lysosomal Signaling Interacts with Mitochondrial ETC to Promote Longevity**

(A–J) Lifespans of *lipl-4 Tg* (A, C, E, G, and I) or *lbp-8 Tg* (B, D, F, H, and J) are examined upon the inactivation of ETC complex I (*nuo-4* RNAi; C and D), complex II (*mev-1* RNAi; E and F), complex III (*isp-1* RNAi; G and H), or complex IV (*cco-1* RNAi; I and J). *lbp-8 Tg* does not enhance the lifespan extension conferred by the inactivation of either complex I, III, or IV ($p > 0.05$, log-rank test). *lipl-4 Tg* further enhances the lifespan extension conferred by the inactivation of complex I or IV ($p < 0.001$, log-rank test) but not III ($p > 0.05$, log-rank test). Neither *lipl-4 Tg* nor *lbp-8 Tg* can extend lifespan with the inactivation of complex II ($p > 0.05$, log-rank test). n = 60–100 for each genotype/condition.

See also Table S1 for lifespan data and Figure S2.

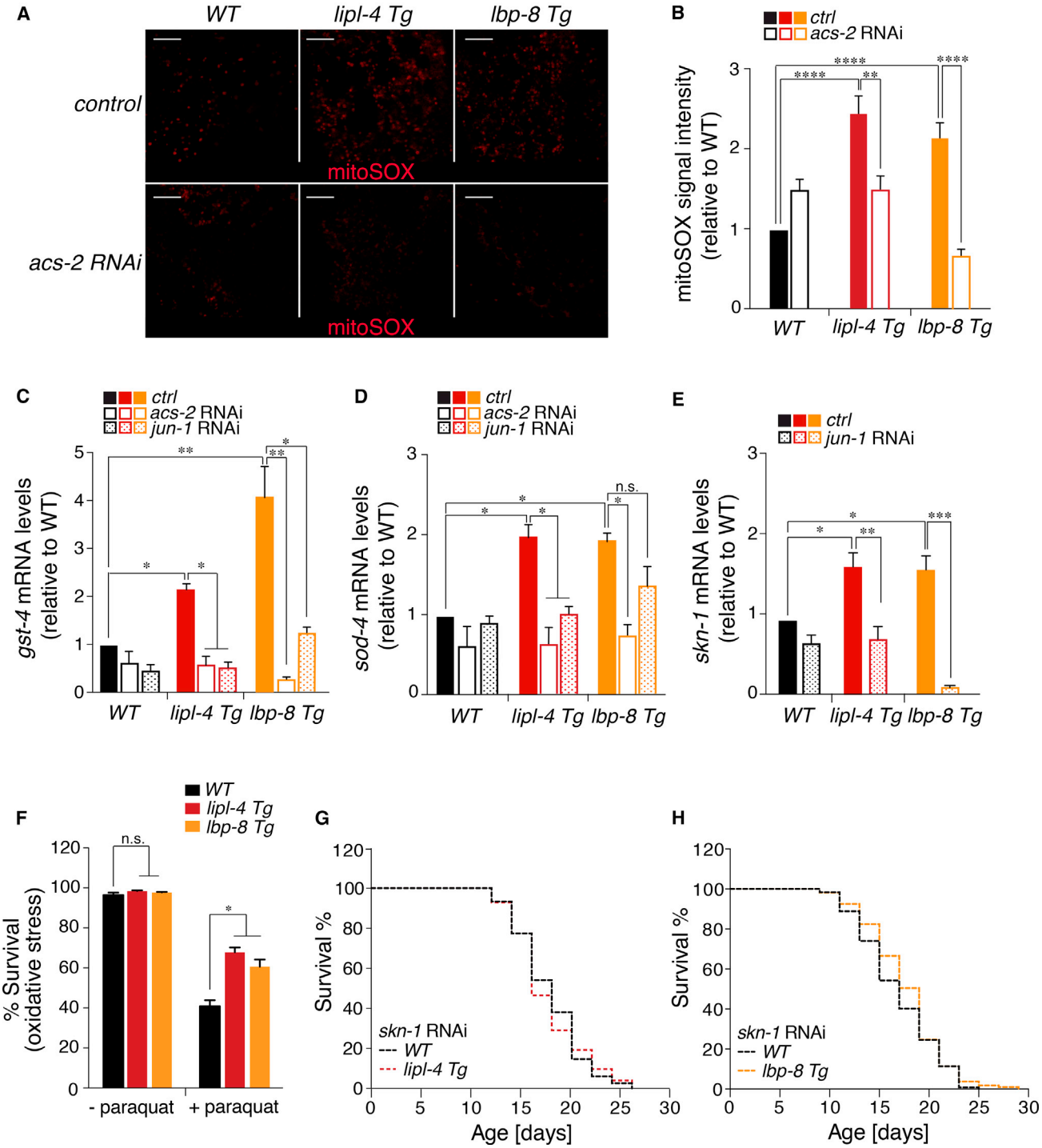


**Figure 6. Lysosomal Pro-longevity Signaling Regulates Redox Homeostasis**

(A and B) Intestines are dissected from WT, *lipl-4 Tg*, and *lbp-8 Tg* adult worms and stained with mitoSOX™ Red. Mitochondrial superoxide levels in *lipl-4 Tg* and *lbp-8 Tg* are increased compared to WT, which is suppressed by *acs-2* RNAi knockdown. Representative images and the quantification of fluorescence intensity are shown in (A) and (B), respectively. n = 20 for each genotype/condition in 3 biological replicates. Error bars represent mean ± SEM. **p < 0.01, ***p < 0.001, one-way ANOVA with Holm-Sidak correction. Scale bar, 70.6 μm.

(C and D) *lipl-4 Tg* and *lbp-8 Tg* show transcriptional induction of oxidative stress responsive genes *gst-4* (C) and *sod-4* (D). The induction of these antioxidant genes is suppressed by RNAi inactivation of the *jun-1* transcription factor or the mitochondrial ß-oxidation gene *acs-2*. n = 1,000 for each genotype/condition in 3 biological replicates. Error bars represent mean ± SEM. n.s. p > 0.05, *p < 0.05, **p < 0.01, one-way ANOVA, Holm-Sidak correction.

*(legend continued on next page)*

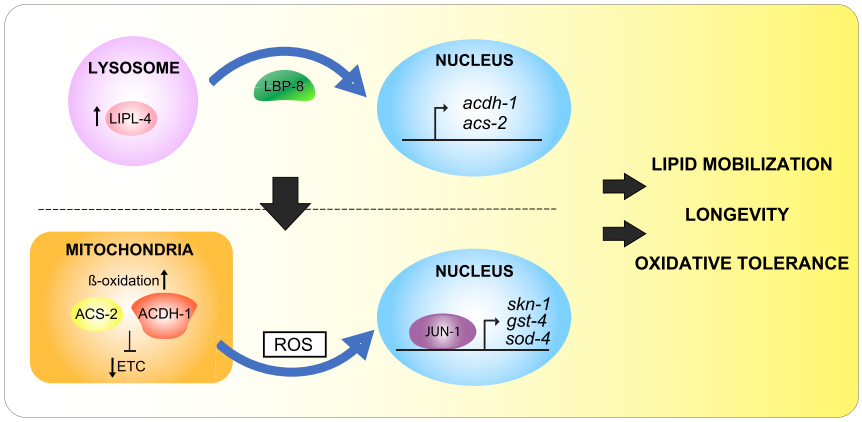


**Figure 7. Summary Model**

Schematic representation of the molecular mechanism by which lysosomal lipid signaling regulates mitochondrial activity and retrograde signaling to improve longevity, metabolic, and redox homeostasis.

observed in other longevity models. For example, long-lived growth hormone receptor knockout mice and Ames dwarf mice both have increased total oxygen consumption and decreased respiratory quotient that varies inversely with lipid oxidation, indicating an induction of energy production by lipid oxidation (Westbrook et al., 2009). Calorie-restricted mice with increased lifespan also have increased fatty acid β-oxidation (Bruss et al., 2010). Further supporting a specific effect of oxidation substrate utilization on longevity, inhibition of glycolysis is sufficient for lifespan extension in *C. elegans* (Schulz et al., 2007). Thus, a preferential utilization of lipid oxidation for energy production is likely associated with an increase in longevity in both *C. elegans* and mammals.

Unlike glycolysis that occurs in the cytoplasm, fatty acid oxidation takes place in mitochondria. Our studies reveal that lysosomal lipolysis actively augments mitochondrial fatty acid β-oxidation via inducing a lysosome-to-nucleus retrograde lipid messenger signaling pathway. This active coordination between lysosomal and mitochondrial metabolic activities can ensure an effective, cooperative catabolic process for maintaining cellular homeostasis and ultimately organism fitness. On the other hand, mitochondria are not only energy hubs of the cell but also centers of cellular signaling (Chandel, 2014; Tait and Green, 2012). Mitochondrial ETC activities can regulate nuclear transcription and epigenetic state in a retrograde fashion by releasing metabolites, proteins, and/or ROS (Chandel, 2015; Durieux et al., 2011; Matilainen et al., 2017; Quirós et al., 2016; Shadel and Horvath, 2015). Previous studies showed that the lifespan extension conferred by the *isp-1* mutation requires the nuclear hormone receptor *nhr-49* (Khan et al., 2013), which controls the expression of *acs-2* (Ratnappan et al., 2014; Van Gilst et al., 2005). Thus, LIPL-4-LBP-8 lysosomal signaling and ETC complex III converge on mitochondrial β-oxidation to promote longevity. Furthermore, mitochondrial β-oxidation is closely coupled with the activity of succinate dehydrogenase in ETC complex II, which oxidizes succinate to fumarate in the citric acid cycle and reduces ubiquinone to ubiquinol in ETC. Succinate dehydrogenase incorporates the cofactor FAD that is also utilized by acyl-CoA dehydrogenase in catalyzing mitochondrial β-oxidation. Given its importance, the catalytic activity of succinate dehydrogenase is subjected to inhibition by acetylation (Cimen et al., 2010) that is induced with increased mitochondrial β-oxidation (Pougovkina et al., 2014). Our results directly reveal that an induction of mitochondrial β-oxidation leads to a reduction in the electron transport activity of succinate dehydrogenase (Figure 3C), which might consequently affect the overall flux through mitochondrial ETC. Thus, there might be a feedforward loop in which the LIPL-4-LBP-8 lysosomal signaling induces mitochondrial β-oxidation, leading to the ETC reduction that further up-regulates mitochondrial β-oxidation.

Mitochondrial ETC complexes I, II, and III are major sites to generate mtROS (Bezawork-Geleta et al., 2017; Wong et al., 2017). In particular, the inhibition of the electron transport from complex II to III can lead to the production of mtROS (Dröse et al., 2009; Quinlan et al., 2012; Yankovskaya et al., 2003). Consistently, our studies reveal that the LIPL-4–LBP-8 lysosomal signaling pathway induces mtROS production and interacts with mitochondrial complex II and III to regulate longevity. mtROS is tightly linked to cellular redox signaling pathways. HIFs can be stabilized by mtROS to induce genes involved in low oxygen adaptation (Chandel et al., 1998; Chandel et al., 2000), and the activation of the JNK signaling pathway by mtROS can turn on oxidative stress responsive genes (Weston and Davis, 2007). Interestingly, mitochondrial retrograde signaling through JUN-1, but not HIF-1, specifically mediates the longevity effect of the lysosomal signaling pathway. Thus, the lysosomal signaling pathway not only adjusts mitochondrial metabolic activity to reprogram catabolic processes but also triggers specific mitochondrial retrograde signaling to improve redox homeostasis. This metabolic and signaling coordination between lysosomes and mitochondria is crucial for promoting metabolic health and longevity and may underlie other longevity mechanisms.

(E) The Nrf2 homolog *skn-1* is transcriptionally induced in *lipl-4 Tg* and *lbp-8 Tg*, which is suppressed by RNAi inactivation of *jun-1*. n = 1,000 for each genotype/condition in 3 biological replicates. Error bars represent mean ± SEM. *p < 0.05, **p < 0.01, ***p < 0.001, one-way ANOVA, Holm-Sidak method.

(F) Compared with WT, *lipl-4 Tg* and *lbp-8 Tg* have increased resistance to oxidative stress induced by paraquat. n = 60–70 for each genotype in 3 biological replicates. Error bars represent mean ± SEM. n.s. p > 0.05, *p < 0.05, two-way ANOVA, Holm-Sidak method.

(G and H) Inactivation of *skn-1* by RNAi fully suppresses the lifespan extension of *lipl-4 Tg* (G) and *lbp-8 Tg* (H) (p < 0.05 *WT* versus *Tg*, log-rank test). n = 60–100 for each genotype/condition.

See also Table S1 for lifespan data.

## STAR★METHODS

Detailed methods are provided in the online version of this paper and include the following:

- KEY RESOURCES TABLE
- CONTACT FOR REAGENT AND RESOURCE SHARING
- EXPERIMENTAL MODEL AND SUBJECT DETAILS
  - *Caenorhabditis elegans* Strains Maintenance
  - Genetic Crosses
  - Bacteria Strains
- METHOD DETAILS
  - Egg Preparation
  - Measurement of Oxygen Consumption Rates and Mitochondrial β-Oxidation Activity
  - Stimulated Raman Scattering (SRS) Microscopy
  - RNA Interference (RNAi) Experiments
  - Lifespan Assays
  - Mitochondrial Enzymology
  - Quantitative RT-PCR
  - Oxidative Stress Resistance Measurement
  - MitoSOX Staining and Imaging
- QUANTIFICATION AND STATISTICAL ANALYSIS

### SUPPLEMENTAL INFORMATION

Supplemental Information includes three figures and two tables and can be found with this article online at https://doi.org/10.1016/j.devcel.2018.12.022.

### ACKNOWLEDGMENTS

We thank J. Sowa and I. Neve for providing OP50 RNAi bacteria; Y. Yu and A. S. Mutlu for SRS support; J. Duffy for providing *raxIs86[lbp-8p::lbp-8::sl2RFP]* transgenic strain; A. Dervisefendic, H. D. Oakley, and P. Svay for maintenance support; and A. S. Mutlu and F. Xia for critical reading of the manuscript. Some strains were obtained from the Caenorhabditis Genetics Center (CGC), which is funded by the NIH Office of Research Infrastructure Programs (P40 OD010440). This work was supported by HHMI (M.C.W.), March of Dimes Foundation (M.C.W.), Welch Foundation (M.C.W.), and National Institutes of Health (R01AG045183, R01AT009050, DP1DK113644; M.C.W.) and by a predoctoral fellowship from the American Heart Association (P.V.R.). We would also like to thank WormBase.

### AUTHOR CONTRIBUTIONS

P.V.R., M.S., A.K.F., B.H.G., and M.C.W. conceived the project. P.V.R., M.S., A.K.F., K.H., and R.M. performed experiments. P.V.R., M.S., A.K.F., and M.C.W. wrote the manuscript.

### DECLARATION OF INTERESTS

The authors declare no competing interests.

Received: December 20, 2017
Revised: September 9, 2018
Accepted: December 27, 2018
Published: January 31, 2019

### REFERENCES

An, J.H., and Blackwell, T.K. (2003). SKN-1 links C. elegans mesendodermal specification to a conserved oxidative stress response. Genes Dev. *17*, 1882–1893.

Balaban, R.S., Nemoto, S., and Finkel, T. (2005). Mitochondria, oxidants, and aging. Cell *120*, 483–495.

Bezawork-Geleta, A., Rohlena, J., Dong, L., Pacak, K., and Neuzil, J. (2017). Mitochondrial Complex II: at the crossroads. Trends Biochem. Sci. *42*, 312–325.

Blackwell, T.K., Steinbaugh, M.J., Hourihan, J.M., Ewald, C.Y., and Isik, M. (2015). SKN-1/Nrf, stress responses, and aging in Caenorhabditis elegans. Free Radic. Biol. Med. *88*, 290–301.

Bruss, M.D., Khambatta, C.F., Ruby, M.A., Aggarwal, I., and Hellerstein, M.K. (2010). Calorie restriction increases fatty acid synthesis and whole body fat oxidation rates. Am. J. Physiol. Endocrinol. Metab. *298*, E108–E116.

Burkewitz, K., Zhang, Y., and Mair, W.B. (2014). AMPK at the nexus of energetics and aging. Cell Metab. *20*, 10–25.

Chandel, N.S. (2015). Evolution of mitochondria as signaling organelles. Cell Metab. *22*, 204–206.

Chandel, N.S., Maltepe, E., Goldwasser, E., Mathieu, C.E., Simon, M.C., and Schumacker, P.T. (1998). Mitochondrial reactive oxygen species trigger hypoxia-induced transcription. Proc. Natl. Acad. Sci. U S A *95*, 11715–11720.

Chandel, N.S. (2014). Mitochondria as signaling organelles. BMC Biol. *12*, 34.

Chandel, N.S., McClintock, D.S., Feliciano, C.E., Wood, T.M., Melendez, J.A., Rodriguez, A.M., and Schumacker, P.T. (2000). Reactive oxygen species generated at mitochondrial complex III stabilize hypoxia-inducible factor-1alpha during hypoxia: a mechanism of O2 sensing. J. Biol. Chem. *275*, 25130–25138.

Cimen, H., Han, M.J., Yang, Y., Tong, Q., Koc, H., and Koc, E.C. (2010). Regulation of succinate dehydrogenase activity by SIRT3 in mammalian mitochondria. Biochemistry *49*, 304–311.

Dillin, A., Hsu, A.L., Arantes-Oliveira, N., Lehrer-Graiwer, J., Hsin, H., Fraser, A.G., Kamath, R.S., Ahringer, J., and Kenyon, C. (2002). Rates of behavior and aging specified by mitochondrial function during development. Science *298*, 2398–2401.

Dröse, S., Hanley, P.J., and Brandt, U. (2009). Ambivalent effects of diazoxide on mitochondrial ROS production at respiratory chain complexes I and III. Biochim. Biophys. Acta *1790*, 558–565.

Durieux, J., Wolff, S., and Dillin, A. (2011). The cell-non-autonomous nature of electron transport chain-mediated longevity. Cell *144*, 79–91.

Felkai, S., Ewbank, J.J., Lemieux, J., Labbé, J.C., Brown, G.G., and Hekimi, S. (1999). CLK-1 controls respiration, behavior and aging in the nematode Caenorhabditis elegans. EMBO J. *18*, 1783–1792.

Feng, J., Bussière, F., and Hekimi, S. (2001). Mitochondrial electron transport is a key determinant of life span in Caenorhabditis elegans. Dev. Cell *1*, 633–644.

Ferrick, D.A., Neilson, A., and Beeson, C. (2008). Advances in measuring cellular bioenergetics using extracellular flux. Drug Discov. Today *13*, 268–274.

Folick, A., Oakley, H.D., Yu, Y., Armstrong, E.H., Kumari, M., Sanor, L., Moore, D.D., Ortlund, E.A., Zechner, R., and Wang, M.C. (2015). Aging. Lysosomal signaling molecules regulate longevity in Caenorhabditis elegans. Science *347*, 83–86.

Hamilton, B., Dong, Y., Shindo, M., Liu, W., Odell, I., Ruvkun, G., and Lee, S.S. (2005). A systematic RNAi screen for longevity genes in C. elegans. Genes Dev. *19*, 1544–1555.

Hansen, M., Hsu, A.L., Dillin, A., and Kenyon, C. (2005). New genes tied to endocrine, metabolic, and dietary regulation of lifespan from a Caenorhabditis elegans genomic RNAi screen. PLoS Genet. *1*, 119–128.

Hansen, M., Rubinsztein, D.C., and Walker, D.W. (2018). Autophagy as a promoter of longevity: insights from model organisms. Nat. Rev. Mol. Cell Biol. *19*, 579–593.

Hiatt, S.M., Duren, H.M., Shyu, Y.J., Ellis, R.E., Hisamoto, N., Matsumoto, K., Kariya, K., Kerppola, T.K., and Hu, C.D. (2009). Caenorhabditis elegans FOS-1 and JUN-1 regulate plc-1 expression in the spermatheca to control ovulation. Mol. Biol. Cell *20*, 3888–3895.

Hwang, A.B., and Lee, S.J. (2011). Regulation of life span by mitochondrial respiration: the HIF-1 and ROS connection. Aging (Albany, NY) *3*, 304–310.

Hwang, A.B., Ryu, E.A., Artan, M., Chang, H.W., Kabir, M.H., Nam, H.J., Lee, D., Yang, J.S., Kim, S., Mair, W.B., et al. (2014). Feedback regulation via AMPK and HIF-1 mediates ROS-dependent longevity in Caenorhabditis elegans. Proc. Natl. Acad. Sci. U S A *111*, E4458–E4467.

Johnson, S.C., Rabinovitch, P.S., and Kaeberlein, M. (2013). mTOR is a key modulator of ageing and age-related disease. Nature *493*, 338–345.

Kennedy, B.K., and Lamming, D.W. (2016). The mechanistic target of rapamycin: the grand conductor of metabolism and aging. Cell Metab. *23*, 990–1003.

Khan, M.H., Ligon, M., Hussey, L.R., Hufnal, B., Farber, R., Munkácsy, E., Rodriguez, A., Dillow, A., Kahlig, E., and Rea, S.L. (2013). TAF-4 is required for the life extension of isp-1, clk-1 and tpk-1 Mit mutants. Aging *5*, 741–758.

Lapierre, L.R., De Magalhaes Filho, C.D., McQuary, P.R., Chu, C.C., Visvikis, O., Chang, J.T., Gelino, S., Ong, B., Davis, A.E., Irazoqui, J.E., et al. (2013). The TFEB orthologue HLH-30 regulates autophagy and modulates longevity in Caenorhabditis elegans. Nat. Commun. *4*, 2267.

Lee, S.J., Hwang, A.B., and Kenyon, C. (2010). Inhibition of respiration extends C. elegans life span via reactive oxygen species that increase HIF-1 activity. Curr. Biol. *20*, 2131–2136.

Lee, S.S., Lee, R.Y., Fraser, A.G., Kamath, R.S., Ahringer, J., and Ruvkun, G. (2003). A systematic RNAi screen identifies a critical role for mitochondria in C. elegans longevity. Nat. Genet. *33*, 40–48.

Levine, B., and Kroemer, G. (2008). Autophagy in the pathogenesis of disease. Cell *132*, 27–42.

Lin, Y.-F., and Haynes, C.M. (2016). Metabolism and the UPR mt. Mol. Cell *61*, 677–682.

Lin, C.J., and Wang, M.C. (2017). Microbial metabolites regulate host lipid metabolism through NR5A-Hedgehog signalling. Nat. Cell Biol. *19*, 550–557.

Luzio, J.P., Pryor, P.R., and Bright, N.A. (2007). Lysosomes: fusion and function. Nat. Rev. Mol. Cell Biol. *8*, 622–632.

Matilainen, O., Quirós, P.M., and Auwerx, J. (2017). Mitochondria and epigenetics - crosstalk in homeostasis and stress. Trends Cell Biol. *27*, 453–463.

McGarry, J.D. (2002). Banting lecture 2001: dysregulation of fatty acid metabolism in the etiology of type 2 diabetes. Diabetes *51*, 7–18.

Neve, I., Sowa, J., and Wang, M. (2015). Modified E. coli B strain OP50 facilitates RNA interference induction in C. elegans. The Worm Breeder's Gazette *20*.

Pellegrino, M.W., Nargund, A.M., and Haynes, C.M. (2013). Signaling the mitochondrial unfolded protein response. Biochim. Biophys. Acta *1833*, 410–416.

Pougovkina, O., te Brinke, H., Ofman, R., van Cruchten, A.G., Kulik, W., Wanders, R.J., Houten, S.M., and de Boer, V.C. (2014). Mitochondrial protein acetylation is driven by acetyl-CoA from fatty acid oxidation. Hum. Mol. Genet. *23*, 3513–3522.

Quinlan, C.L., Orr, A.L., Perevoshchikova, I.V., Treberg, J.R., Ackrell, B.A., and Brand, M.D. (2012). Mitochondrial complex II can generate reactive oxygen species at high rates in both the forward and reverse reactions. J. Biol. Chem. *287*, 27255–27264.

Quirós, P.M., Mottis, A., and Auwerx, J. (2016). Mitonuclear communication in homeostasis and stress. Nat. Rev. Mol. Cell Biol. *17*, 213–226.

Rajawat, Y.S., Hilioti, Z., and Bossis, I. (2009). Aging: central role for autophagy and the lysosomal degradative system. Ageing Res. Rev. *8*, 199–213.

Ramachandran, P.V., Mutlu, A.S., and Wang, M.C. (2015). Label-free biomedical imaging of lipids by stimulated Raman scattering microscopy. Curr. Protoc. Mol. Biol. *109*, 30.3.1–30.3.17.

Randle, P.J. (1998). Regulatory interactions between lipids and carbohydrates: the glucose fatty acid cycle after 35 years. Diabetes Metab. Rev. *14*, 263–283.

Ratnappan, R., Amrit, F.R., Chen, S.W., Gill, H., Holden, K., Ward, J., Yamamoto, K.R., Olsen, C.P., and Ghazi, A. (2014). Germline signals deploy NHR-49 to modulate fatty-acid beta-oxidation and desaturation in somatic tissues of C. elegans. PLoS Genet. *10*, e1004829.

Ristow, M., and Zarse, K. (2010). How increased oxidative stress promotes longevity and metabolic health: the concept of mitochondrial hormesis (mitohormesis). Exp. Gerontol. *45*, 410–418.

Saxton, R.A., and Sabatini, D.M. (2017). MTOR signaling in growth, metabolism, and disease. Cell *168*, 960–976.

Schulz, T.J., Zarse, K., Voigt, A., Urban, N., Birringer, M., and Ristow, M. (2007). Glucose restriction extends Caenorhabditis elegans life span by inducing mitochondrial respiration and increasing oxidative stress. Cell Metab. *6*, 280–293.

Sena, L.A., and Chandel, N.S. (2012). Physiological roles of mitochondrial reactive oxygen species. Mol. Cell *48*, 158–167.

Settembre, C., Fraldi, A., Medina, D.L., and Ballabio, A. (2013). Signals from the lysosome: a control centre for cellular clearance and energy metabolism. Nat. Rev. Mol. Cell Biol. *14*, 283–296.

Shadel, G.S., and Horvath, T.L. (2015). Mitochondrial ROS signaling in organismal homeostasis. Cell *163*, 560–569.

Tait, S.W., and Green, D.R. (2012). Mitochondria and cell signalling. J. Cell Sci. *125*, 807–815.

Uno, M., Honjoh, S., Matsuda, M., Hoshikawa, H., Kishimoto, S., Yamamoto, T., Ebisuya, M., Yamamoto, T., Matsumoto, K., and Nishida, E. (2013). A fasting-responsive signaling pathway that extends life span in C. elegans. Cell Rep. *3*, 79–91.

Van Gilst, M.R., Hadjivassiliou, H., Jolly, A., and Yamamoto, K.R. (2005). Nuclear hormone receptor NHR-49 controls fat consumption and fatty acid composition in C. elegans. PLoS Biol. *3*, e53.

Wang, M.C., Bohmann, D., and Jasper, H. (2003). JNK signaling confers tolerance to oxidative stress and extends lifespan in Drosophila. Dev. Cell *5*, 811–816.

Wang, M.C., O'rourke, E.J., and Ruvkun, G. (2008). Fat metabolism links germline stem cells and longevity in C. elegans. Science *322*, 957–960.

Wang, M.C., Min, W., Freudiger, C.W., Ruvkun, G., and Xie, X.S. (2011). RNAi screening for fat regulatory genes with SRS microscopy. Nat. Methods *8*, 135–138.

Wang, Y., and Hekimi, S. (2015). Mitochondrial dysfunction and longevity in animals: untangling the knot. Science *350*, 1204–1207.

Westbrook, R., Bonkowski, M.S., Strader, A.D., and Bartke, A. (2009). Alterations in oxygen consumption, respiratory quotient, and heat production in long-lived GHRKO and Ames dwarf mice, and short-lived bGH transgenic mice. J. Gerontol. A Biol. Sci. Med. Sci. *64*, 443–451.

Weston, C.R., and Davis, R.J. (2007). The JNK signal transduction pathway. Curr. Opin. Cell Biol. *19*, 142–149.

Wong, H.S., Dighe, P.A., Mezera, V., Monternier, P.A., and Brand, M.D. (2017). Production of superoxide and hydrogen peroxide from specific mitochondrial sites under different bioenergetic conditions. J. Biol. Chem. *292*, 16804–16809.

Yang, W., and Hekimi, S. (2010). Two modes of mitochondrial dysfunction lead independently to lifespan extension in Caenorhabditis elegans. Aging Cell *9*, 433–447.

Yankovskaya, V., Horsefield, R., Törnroth, S., Luna-Chavez, C., Miyoshi, H., Léger, C., Byrne, B., Cecchini, G., and Iwata, S. (2003). Architecture of succinate dehydrogenase and reactive oxygen species generation. Science *299*, 700–704.

Yu, Y., Ramachandran, P.V., and Wang, M.C. (2014). Shedding new light on lipid functions with CARS and SRS microscopy. Biochim. Biophys. Acta *1841*, 1120–1129.

# STAR★METHODS

## KEY RESOURCES TABLE

| REAGENT or RESOURCE | SOURCE | IDENTIFIER |
|---|---|---|
| Bacterial and Virus Strains | | |
| RNAi feeding strain | Caenorhabditis Genetics Center | HT115(DE3) |
| RNAi feeding strain | (Neve et al., 2015) | OP50 |
| Vidal RNAi library | Open Biosystems | ORF RNAi Collection V1.1 |
| Ahringer RNAi library | Source BioScience | *C. elegans* RNAi Collection (Ahringer) |
| Chemicals, Peptides, and Recombinant Proteins | | |
| Etomoxir sodium salt | Sigma-Aldrich | E1905-5MG |
| $NaN_3$ | Sigma-Aldrich | S2002 |
| NADH | Sigma-Aldrich | 10128023001 |
| Potassium ferricyanide | Sigma-Aldrich | 702587 |
| Succinate | Sigma-Aldrich | S2378 |
| DCIP | Sigma-Aldrich | D1878 |
| Rotenone | Sigma-Aldrich | 45656 |
| Potassium cyanide | Sigma-Aldrich | 60178 |
| Decylubiquinone | Sigma-Aldrich | D7910 |
| Cytochrome c | Sigma-Aldrich | C2037 |
| DTNB | Sigma-Aldrich | D218200 |
| Acetyl-CoA | Sigma-Aldrich | 10101893001 |
| Oxaloacetate | Sigma-Aldrich | O4126 |
| Paraquat | Sigma-Aldrich | 36541 |
| MitoSOX Red | ThermoFischer | M36008 |
| Carbenicillin | Sigma-Aldrich | C1389 |
| Tetracycline | Sigma-Aldrich | 87128 |
| IPTG | Research Products Int. | 156000 |
| Critical Commercial Assays | | |
| SuperScript III First-Strand Synthesis System | Invitrogen | 18080051 |
| RNA column purification | Qiagen | 74104 |
| Kapa SYBR fast PCR kit | KAPA Biosystems | KK4602 |
| Experimental Models: Organisms/Strains | | |
| *C. elegans* N2 Bristol | CGC | N2 |
| (*isp-1(qm150)*) | CGC | MQ887 |
| (*clk-1(qm30)*) | CGC | MQ130 |
| *raxIs3[ges-1p::lipl-4::sl2gfp]* | (Folick et al., 2015) | MCW74 |
| *raxEx32[lbp-8p::lbp-8::sl2gfp]* | (Folick et al., 2015) | MCW213 |
| *raxIs4[lbp-8p::lbp-8::sl2gfp]* | (Folick et al., 2015) | MCW146 |
| *raxIs86[lbp-8p::lbp-8::3xflag::SL2RFP; myo-2p::GFP]* | This paper | MCW897 |
| *raxEx354[ges-1p::acs-2::sl2rfp]* | This paper | MCW1061 |
| Oligonucleotides | | |
| *rpl-32* FWD AGGGAATTGATAACCGTGTCCGCA | (Wang et al., 2008) | N/A |
| *rpl-32* REV TGTAGGACTGCATGAGGAGCATGT | (Wang et al., 2008) | N/A |
| *sod-4* FWD ATATTGAGTCACCGGCTTCC | This paper | N/A |
| *sod-4* REV TAACCACACTTCGGCCAAT | This paper | N/A |
| *gst-4* FWD ATGCTCGTGCTCTTGCTGAG | This paper | N/A |
| *gst-4* REV GGAGTCGTTGGCTTCAGCTT | This paper | N/A |
| *hsp-6* FWD AGC CAAGTTCGAGCAGATTG | This paper | N/A |

(*Continued on next page*)

**Continued**

| REAGENT or RESOURCE | SOURCE | IDENTIFIER |
|---|---|---|
| *hsp-6* REV TTGCACCTTTGGCATTCTGC | This paper | N/A |
| *hsp-60* FWD CCAAGGACGTCAAGTTCGGA | This paper | N/A |
| *hsp-60* REV CCACGACTGCTCGATGATCA | This paper | N/A |
| *nduo-1* FWD AGCGTCATTTATTGGGAAGAAGAC | (Lin and Wang, 2017) | N/A |
| *nduo-1* REV AAGCTTGTGCTAATCCCATAAATGT | (Lin and Wang, 2017) | N/A |
| *ctb-1* FWD ATTGCCGTGAGCTATTCTAGTT | (Lin and Wang, 2017) | N/A |
| *ctb-1* REV ACCGTGGCAATATAACCTAGATG | (Lin and Wang, 2017) | N/A |
| *skn-1* FWD CTTCGGAATCTCCACGATACAC | This paper | N/A |
| *skn-1* REV ACTGGATGGAGCCAACTTTC | This paper | N/A |
| *acdh-1* FWD GCGGATGGTCTTACTGTAGATAAGG | This paper | N/A |
| *acdh-1* REV GACACGAACATTGTCAAAATGAACT | This paper | N/A |
| *acdh-2* FWD ATGCAAACAGTCGCCAAAA | This paper | N/A |
| *acdh-2* REV CTTTCTCAGGATCCGCATTT | This paper | N/A |
| *acdh-3* FWD CTACCATGTCTACGAAGCCTC | This paper | N/A |
| *acdh-3* REV GTCCATTTCACGAACAAGCG | This paper | N/A |
| *acdh-4* FWD CTTGGTGTTTGCTAATGCGG | This paper | N/A |
| *acdh-4* REV ATGAAGTGGGCACGTAGAAG | This paper | N/A |
| *acdh-7* FWD CACCGCATTTGTCGTTGAAG | This paper | N/A |
| *acdh-7* REV TCGTTGTCCCATGTTGATCTC | This paper | N/A |
| *acdh-8* FWD TGTTGGCTGCTGAACCTATC | This paper | N/A |
| *acdh-8* REV GCATGTCCTCCACCAGTAATC | This paper | N/A |
| *acdh-10* FWD GTGGAGATGTTTGGACGAGTC | This paper | N/A |
| *acdh-10* REV TGGCGGATTTGTAGGTGATAAG | This paper | N/A |
| *acdh-5* FWD TGTATCGAACTGTTCTGGCAC | This paper | N/A |
| *acdh-5* REV TTCAAATATCCTGCACCTCCC | This paper | N/A |
| *acdh-6* FWD ACCCGTTCTTTGCTCTATCG | This paper | N/A |
| *acdh-6* REV TTTCAATTTCGCCATCGCAG | This paper | N/A |
| *acdh-12* FWD TCGTCAATATGAGATGCACCG | This paper | N/A |
| *acdh-12* REV TGTTCTTGATGGCATAGGTGG | This paper | N/A |
| *jun-1* FWD GCGACAGGATATGGAAGTAGATG | This paper | N/A |
| *jun-1* REV GGGAGAACTGGAGATGAAACAG | This paper | N/A |
| Software and Algorithms | | |
| ImageJ | | ImageJ 1.51f, http://fiji.sc/ |
| Illustrator | Adobe | Version CC 2015 |
| GraphPad Prism 5 | GraphPad Software | https://www.graphpad.com/scientificsoftware/prism/ |
| SPSS | IBM | https://www.ibm.com/analytics/academic-statistical-software |

## CONTACT FOR REAGENT AND RESOURCE SHARING

Further information and requests for resources and reagents should be directed to and will be fulfilled by the Lead Contact, Meng C. Wang (wmeng@bcm.edu).

## EXPERIMENTAL MODEL AND SUBJECT DETAILS

### *Caenorhabditis elegans* Strains Maintenance

*C. elegans* strains used in this study are listed in the Key Resources Table. The following strains were obtained from the Caenorhabditis Genetics Center (CGC): Wild-type (N2), MQ887 (*isp-1(qm150)*), MQ130 (*clk-1(qm30)*). The following transgenic strains

were generated in the lab: *raxIs3[ges-1p::lipl-4::sl2gfp], raxEx32[lbp-8p::lbp-8::sl2gfp], raxIs4[lbp-8p::lbp-8::sl2gfp], raxIs86[lbp-8p::lbp-8::sl2gfp]*. Generation of transgenic strains was described previously (Folick et al., 2015). The strains were maintained and experiments performed at 20°C, except oxygen consumption and mitochondrial β-oxidation measurements which were performed at room temperature. Strains were maintained on standard nematode growth medium (NGM) plates seeded with corresponding bacteria. When nematodes were prepared for experimentation, gravid adults were bleached with sodium hypochlorite to collect fresh embryos using the method described below.

### Genetic Crosses

Genetic crosses were performed using standard methods. *lipl-4 Tg* or *lbp-8 Tg* transgenic males were generated by crossing N2 males to the transgenic strains that carry fluorescence markers. The transgenic males with the fluorescence markers were then crossed to the desired strain. For *lipl-4 Tg* crosses, the *raxIs3[ges-1p::lipl-4::sl2gfp]* strain was used for crossing to MQ887 and MQ130. For the *lbp-8 Tg* crosses, *raxIs4[lbp-8p::lbp-8::sl2gfp]* was crossed to MQ887. The *raxIs4* strain carries a transgene insertion at a close proximity to the *clk-1* gene on chromosome III, and could not be crossed to MQ130. Thus, the extrachromosomal array-containing strain, *raxEx32[lbp-8p::lbp-8::sl2gfp]* that was used to generate *raxIs4*, was used for the cross with MQ130. Longitudinal survival analysis or other measurements were performed by comparing transgene-containing strains to their non-transgenic siblings generated from the same cross.

### Bacteria Strains

A single colony of *E. coli* OP50 was cultured in lysogeny broth (LB) at 37°C shaking overnight with 100 μg/mL streptomycin. 300 μL of OP50 was seeded and dried on petri dishes containing NGM. RNAi OP50 or HT115 colonies were selected by carbenicillin (50 μg $ml^{-1}$) and tetracycline (50 μg $ml^{-1}$) resistance, cultured for 14 h or 18 h respectively, and verified by Sanger sequencing. Bacteria containing L4440 vector were used as empty vector controls for RNAi experiments.

## METHOD DETAILS

### Egg Preparation

Worms were grown to adulthood in petri dishes containing NGM *E. coli* OP50 or HT115. Gravid adults were collected in a 15 mL conical tube with 10 mL of M9 minimal medium (22mM $KH_2PO_4$ , 22mM $Na_2HPO_4$, 85mM NaCl, 2mM $MgSO_4$). A bleach solution (60% NaOCl, 1.6M NaOH solution) was freshly prepared. Worms were spun down in a centrifuge for 30 seconds at 3000 RPM and M9 was aspirated. 2 mL of bleach was added to each aliquot of adult worms. Worm bodies were dissolved in the conical tube by shaking for 1 minute, and repeating this step twice more. Embryos and dissolved worm bodies were immediately spun and the bleach solution was aspirated. Embryos were rinsed 4 times by adding 10 mL of M9 to each tube, by spinning, and aspirating. Embryos were allowed to hatch overnight on a shaker in 6 mL of M9.

### Measurement of Oxygen Consumption Rates and Mitochondrial β-Oxidation Activity

Oxygen consumption rates were measured on whole worms using ten samples each for N2 and *lipl-4 Tg* using the XF24 Extracellular Flux Analyzer (Seahorse Bioscience). Measurements were performed at room temperature (26.9°C with heat generated by the machine). Age-synchronized worms were grown on *E. coli* OP50 NGM plates and collected as young adults. The worms were washed in M9 buffer twice, and approximately 200 animals for each sample were added in 500 μl M9 buffer to the XF24 plate, and ten technical replicates were measured. The oxygen consumption rate was measured three times at baseline and three times after the addition of etomoxir sodium salt (Sigma-Aldrich), an inhibitor of mitochondrial β-oxidation via carnitine palmitoyltransferase 1, dissolved in M9 to a 500 μM final concentration. For each well, the percent change in the average oxygen consumption rate before and after etomoxir addition was used to calculate the oxygen consumption rate dependent on mitochondrial fatty-acid β-oxidation as described previously (Ferrick et al., 2008). Comparisons were made between samples run in parallel on the same plate and repeated in three independent biological replicates. This method using whole worms might represent a limitation for differences in mitochondrial physiology due to the animal motility. So, we have used the mean of ten technical replicates for one biological replicate, and the variation among three independent biological replicates is minor.

### Stimulated Raman Scattering (SRS) Microscopy

For comparison of total lipid storage in *lipl-4 Tg* and *lbp-8 Tg* versus N2, day-1 adult worms were used. Worms were mounted on glass slides with 2% agarose pads containing 0.5% $NaN_3$ as anesthetic. Label-free lipid SRS imaging was performed as previously described (Wang et al., 2011). Pump (tunable from 780 nm to 990 nm) and Stokes (1064 nm) laser beams from *pico*EMERALD one-box laser (Applied Physics and Electronics, Germany) were coupled into a modified laser scanning confocal microscope (IX81/FV1000, Olympus) optimized for near-infrared throughput. A 20X air objective and an air condenser were used. For imaging lipids, we used 815.7 nm pump laser and 1064 nm Stokes laser based on the Raman shift of $CH_2$ chemical bonds (2,845 $cm^{-1}$). A single z-slice with the nuclei of the first anterior pair of intestinal cells in focus was selected for imaging. SRS signal intensity is proportional to the fat content level (Ramachandran et al., 2015; Wang et al., 2011; Yu et al., 2014). Images were analyzed using

ImageJ (NIH). The average pixel intensity of SRS signals in the area of the first anterior pair of intestinal cells was quantified and normalized to N2 or vehicle-treated controls.

### RNA Interference (RNAi) Experiments

RNAi clones from the libraries generated in the laboratories of Dr. Julie Ahringer and Dr. Marc Vidal were used. All the RNAi clones were confirmed using Sanger sequencing. For knockdown of *acs-2* and *acdh-1*, the corresponding dsRNA plasmid from the Ahringer library was transformed into genetically modified competent OP50 cells [rnc14::DTn10 laczgA::T7pol camFRT], which lack RNAIII RNase activity but gain IPTG-inducible T7 RNA polymerase (Neve et al., 2015). RNAi OP50 colonies were selected by carbenicillin (50 $\mu g\ ml^{-1}$) and tetracycline (50 $\mu g\ ml^{-1}$) resistance and verified by Sanger sequencing. All the other RNAi-based experiments were performed with HT115 bacteria. Bacteria containing L4440 vector were used as empty vector controls.

### Lifespan Assays

Worms were age-synchronized by bleach-based egg isolation followed by starvation in M9 buffer at the L1 stage for at least 24 hours. For all experiments, every genotype and condition was performed in parallel. Synchronized L1 worms were grown to the first day of adulthood, and Day 0 of the lifespan was determined by the onset of egg-laying. During adulthood, worms were transferred to new plates every two days. 60-100 animals were assayed for each condition/genotype with 30-40 animals per 6 cm plate. Death was indicated by total cessation of movement in response to gentle mechanical stimulation. For integrated transgenic strains, the strain was backcrossed to N2 more than ten times prior to lifespan analysis.

### Mitochondrial Enzymology

For enzyme assays of electron transport chain complexes (ETC) I-IV, 20,000 age-synchronized day-1 hermaphrodite adult worms were used per sample. Worms were washed 3 times in PBS and flash-frozen in minimal liquid. Homogenization buffer (120 mM KCl, 20mM HEPES, 1mM EGTA, pH 7.4) was added to a final volume of 200 $\mu L$ and the worms were sonicated (5 second pulse x4, 60% power) using a Microson XL2000 Ultrasonic Cell Disruptor (Misonix). All samples were diluted to a final concentration of 1 $\mu g/\mu l$ of protein. The spectrophotometric kinetic assays were performed at 25°C using a monochromator microplate reader (Tecan M200). Complex I activity (NADH:ubiquinone oxidoreductase) was determined by measuring oxidation of NADH at 340 nm (using ferricyanide as the electron acceptor) in a reaction mixture of 50 mM potassium phosphate (pH 7.5), 0.2 mM NADH, and 1.7 mM potassium ferricyanide. Complex II activity (succinate dehydrogenase) was determined by measuring the reduction of the artificial electron acceptor 2,6-dichlorophenol-indophenol (DCIP) at 600 nm in a reaction mixture of 50 mM potassium phosphate (pH 7.5), 20 mM succinate, 2 $\mu M$ DCIP, 10 $\mu M$ rotenone, and 1 mM potassium cyanide. Complex III activity (ubiquinol:cytochrome c oxidoreductase) was determined by measuring the reduction of cytochrome c at 550 nm in a reaction mixture of 50 mM potassium phosphate (pH 7.5), 35 $\mu M$ reduced decylubiquinone, 15 $\mu M$ cytochrome c, 10 $\mu M$ rotenone, and 1 mM potassium cyanide. Complex IV activity (cytochrome c oxidase) was determined by measuring the oxidation of cytochrome c at 550 nm in a reaction mixture of 50 mM potassium phosphate (pH 7.0) and 100 $\mu M$ reduced cytochrome c. Citrate synthase activity was determined by measuring the reduction of 5,5'-dithiobis (2-nitrobenzoic acid) (DTNB) at 412 nm which is coupled to the reduction of acetyl-CoA by citrate synthase in the presence of oxaloacetate. The reaction mixture consists of 100 mM Tris-HCl (pH 8.0), 100 $\mu M$ DTNB, 50 $\mu M$ acetyl-CoA, and 425 $\mu M$ oxaloacetate. All activities were calculated as nmoles/min/mg protein, normalized to citrate synthase activity and finally expressed as percentage of wild type activity.

### Quantitative RT-PCR

Total RNA was isolated from at least 1000 age-synchronized young adult worms by Trizol® extraction followed by column purification (Qiagen). Synthesis of cDNA was performed using the SuperScript III First-Strand Synthesis System (Invitrogen). Quantitative PCR was performed using Kapa SYBR fast PCR kit (Kapa Biosystems) in a Realplex 4 PCR machine (Eppendorf), and values were normalized to *rpl-32* as an internal control. All data shown represent three biologically independent samples. Primers used in this study are listed in the Key Resources Table.

### Oxidative Stress Resistance Measurement

Age-synchronized day-1 hermaphrodite adult worms were washed off NGM plates, rinsed three times with M9 buffer, and 60-70 worms were seeded to each well on a 24-well plate. Animals were subjected to oxidative stress using 100mM paraquat in M9 (Sigma #856177) for 6 hours, following by survivability measurements. 6 replicates were used for each genotype/condition.

### MitoSOX Staining and Imaging

MitoSOX Red (Thermo Fischer, M36008) can react with mitochondrial oxidants and superoxide exhibiting red fluorescence. Due to the low cuticle permeability of mitoSOX in *C. elegans*, we dissected intestine from WT, *lipl-4 Tg* and *lbp-8 Tg* adult worms prior staining. We transferred the dissected tissues into the mitoSOX Red staining solution freshly prepared before each use (5 $\mu M$ in M9, prepared from a 5 mM stock in DMSO) and incubate in the dark for 15 minutes at room temperature. Stained tissues were washed three times with M9 before imaging using 510 nm excitation laser. Confocal images were taken using an FV1000 microscope (Olympus). Twenty worms were used for each genotype/condition in three different biological replicates.

## QUANTIFICATION AND STATISTICAL ANALYSIS

All comparisons of means were accomplished using a one-way ANOVA, two-way ANOVA and two sample unpaired t-test using Holm-Sidak correction as indicated in the corresponding figure legends. For all figure legends, asterisks indicate statistical significance as follows: n.s. = not significant $p>0.05$; * $p<0.05$, ** $p<0.01$, *** $p<0.001$. Data were obtained by performing independently three biological replicates. Figures and graphs were constructed using GraphPad Prism 5 (GraphPad Software) and Illustrator (CC 2015; Adobe). For the lifespan analysis statistical analyses were performed with SPSS (IBM Software) using Kaplan-Meier survival analysis and the log-rank test.